ChemCatChem

ChemCatChem
Chemistry Europe
European Chemical Societies Publishing

RESEARCH ARTICLE OPEN ACCESS

Efficient Room-Temperature Methane Oxidation by μ-Nitrido-Bridged Iron Phthalocyanine Dimer Deposited on Conductive Carbon Black

Yasuyuki Yamada[1,2,3] | Akiko Sakata[2] | Yuka Toyoda[2] | Chaoqi Chen[1,2] | Satoshi Muratsugu[1,3] | Yutaka Hitomi[4] | Kin-ichi Oyama[2] | Akiyoshi Kuzume[5] | Koji Harano[6,7] | Mizuki Tada[1,2,3] | Kentaro Tanaka[1,3,8]

[1]Department of Chemistry, Graduate School of Science, Nagoya University, Nagoya, Japan | [2]Research Center for Materials Science, Nagoya University, Nagoya, Japan | [3]Integrated Research Consortium on Chemical Sciences, Nagoya University, Nagoya, Japan | [4]Department of Molecular Chemistry and Biochemistry, Graduate School of Science and Engineering, Doshisha University, Kyotanabe, Kyoto, Japan | [5]Clean Energy Research Centre, University of Yamanashi, Yamanashi, Japan | [6]Center for Basic Research on Materials, National Institute for Materials Science, Tsukuba, Japan | [7]Research Center for Autonomous Systems Materialogy (ASMat), Institute of Integrated Research, Institute of Science Tokyo, Yokohama, Japan | [8]Research Institute for Quantum and Chemical Innovation, Institute of Innovation for Future Society, Nagoya University, Nagoya, Japan

Correspondence: Yasuyuki Yamada (yamada.yasuyuki.i6@f.mail.nagoya-u.ac.jp) | Kentaro Tanaka (kentaro@chem.nagoya-u.ac.jp)

Received: 3 September 2025 | **Revised:** 21 December 2025 | **Accepted:** 12 January 2026

Keywords: μ-nitrido-bridged dimer | carbon substrate | iron phthalocyanine | methane oxidation | room temperature

ABSTRACT

Appropriate deposition of metal complex-based catalysts on solid carriers sometimes results in considerably higher catalytic activity than that of the metal complex alone, due to interactions between the complex and the solid. These catalysts could be a part of single-molecule catalysts (SMCs) or site-isolated molecular complex catalysts (SIMCs). Herein, we report a solid-supported metal complex catalyst for CH_4 oxidation at room temperature. Specifically, μ-nitrido-bridged iron phthalocyanine dimer deposited on conductive carbon black can oxidatively activate the chemically stable C—H bond of CH_4 with high efficiency even at 25°C in an aqueous solution containing H_2O_2 as an oxidant. Its catalytic activity for CH_4 oxidation is much higher than that of the commonly used Fenton reaction with Fe^{2+} and H_2O_2 under the same conditions. Such high catalytic oxidizing activity is attributable to the interaction between the specific surface sites of carbon black and the high-valent iron-oxo species of the catalyst molecule.

1 | Introduction

By atomically dispersing isolated metal ions on solid carriers, single-atom catalysts (SACs) have shown outstanding activity in a variety of reactions due to their high density of active sites [1–7]. Similarly, single-molecule catalysts (SMCs) [8] and site-isolated molecular complex catalysts (SIMCs) [9] can be constructed by dispersing and immobilizing metal complexes on solid carriers. In these catalysts, the metal center coordinated by ligands functions as a "single site." There are two practical ways to tune the catalytic activity of SMCs and SIMCs: (i) ligand design of the metal complex deposited on the solid surface, and (ii) tuning the electronic state of the metal center through interaction with the solid support. An appropriate combination of coordinating ligand and solid support in SMCs or SIMCs would result in a better catalytic performance than that of the conventional metal complex-based homogeneous catalysts. In particular, carbon-based supports are extremely promising for SMCs or SIMCs due to their mechanical and electrochemical stability, high specific surface area, porous structure, and easy introduction of defects or substituents, including various heteroatoms such as O, N, and B [10–12].

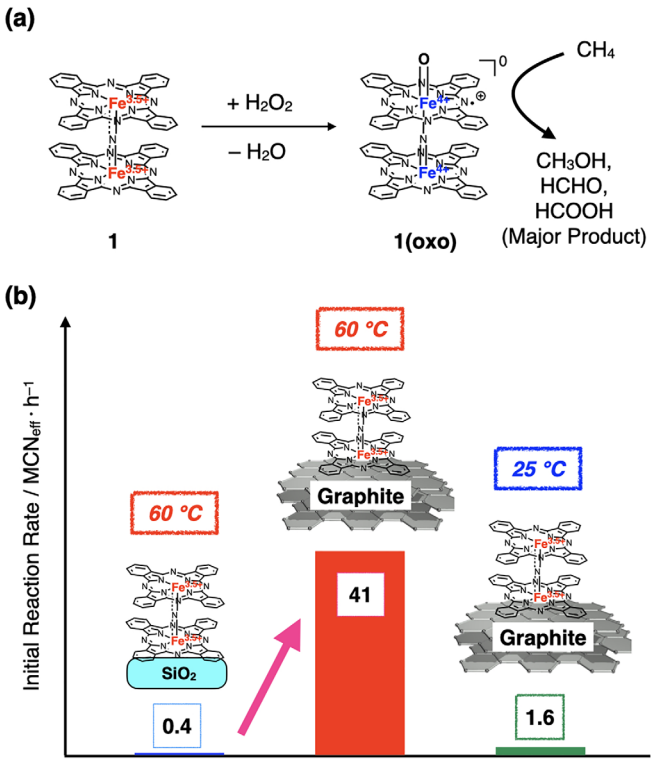

FIGURE 1 | Catalytic CH_4 oxidation by μ-nitrido-bridged iron phthalocyanine-based catalysts. (a) Production of high-valent iron-oxo species (**1(oxo)**) applicable to CH_4 oxidation through the reaction of μ-nitrido-bridged iron phthalocyanine dimer **1** and H_2O_2. (b) Comparison of the initial CH_4 oxidation rate based on the effective methane conversion number MCN_{eff} of **1** supported on SiO_2 (**1**/SiO_2) and graphite (**1**/G) at 60°C and 25°C in an acidic aqueous solution using H_2O_2 as an oxidant [36].

This paper reports an efficient room-temperature CH_4 oxidation reaction enabled by a highly dispersed metal complex-based catalyst on the surface of a conductive carbon support. Since CH_4 is abundant in natural gas, shale gas, and methane hydrate, efficient catalytic activation of its C—H bond will expand its role as a carbon source for producing chemicals [13–16]. Nevertheless, this activation remains difficult because CH_4 has a high bond dissociation energy (104.9 kcal/mol), low polarizability, and negligible electron affinity. Therefore, although catalysts enabling low-temperature C—H activation of CH_4 are indispensable [13–16], only a few catalysts have achieved this at room temperature [17–25, 30]. For instance, Cui et al. demonstrated room-temperature oxidative C—H bond activation of CH_4 by Fe-carbon-based SAC, using H_2O_2 as an oxidizing reagent [21].

We hypothesize that novel SMCs or SIMCs could be used to prepare efficient catalysts for room-temperature CH_4 conversion. Specifically, we chose a μ-nitrido-bridged iron phthalocyanine dimer **1** as the molecular part. The high-valent terminal iron-oxo species **1(oxo)**, produced through the reaction of **1** with H_2O_2, is known to possess particularly potent oxidation ability among various artificial metal complex-based oxidation catalysts (Figure 1a) [31–33]. High-valent iron-oxo species such as **1(oxo)** can activate stable C—H bonds via a proton-coupled electron transfer (PCET) mechanism, followed by radical recombination to afford hydroxylated compounds [34, 35]. As a result, **1** can catalytically activate the C—H bond of CH_4 in acidic aqueous solutions containing excess H_2O_2 at below 100°C to produce the oxidized products (mainly formic acid, and also methanol and formaldehyde) [31–33]. Moreover, we recently found that stacking **1** on a graphite surface (**1**/G) significantly enhanced its ability to catalytically oxidize CH_4 compared to the silica-supported counterpart (**1**/SiO_2), as evidenced by a much higher MCN_{eff} value (to be defined later) of 1.1×10^{-2} s^{-1} for **1**/G versus 1.1×10^{-4} s^{-1} for **1**/SiO_2 at 60°C in an acidic aqueous solution (Figure 1b) [36]. These results are apparently due to the benefits of SMC (or SIMC). However, the catalytic CH_4 oxidation performance of **1**/G at room temperature (25°C) was still very low ($MCN_{eff} = 4.4 \times 10^{-4}$ s^{-1}). Hence, it is desirable to develop a strategy to dramatically improve the catalytic activity of **1**/G.

Assuming that the graphite support in **1**/G can tune the catalytic activity of **1** in this SMC (or SIMC), a different solid support may improve the performance. Conductive carbon black is a good candidate for this purpose, because it possesses a large π-plane surface for efficient interaction with **1** and **1(oxo)**, even though its structure is considerably different from that of graphite by including a number of defects and substituents such as –COOH, –CHO, and –OH [37, 38]. Here, we dispersed **1** on conductive carbon blacks such as Vulcan XC-72R in order to improve the catalytic C—H bond activation of CH_4 at room temperature.

2 | Results and Discussion

2.1 | Preparation and Characterization of Vulcan XC-72R-Supported Catalyst

In its neutral form, the μ-nitrido-bridged iron phthalocyanine dimer with no peripheral substituents (**1**) is poorly soluble in many organic solvents, making it difficult to prepare supported catalysts. However, we recently developed a method to efficiently assemble **1** on a graphite surface by using its $1e^-$-oxidized monocationic complex ($\mathbf{1}^+ \cdot I^-$). Heating graphite (1.0 g) with $\mathbf{1}^+ \cdot I^-$ (8.0 mg, 5.7 μmol) in pyridine at 80°C for 24 h quantitatively produced the desired catalyst **1**/G, in which **1** was stacked on the graphite surface [36]. Pyridine is a good solvent for $\mathbf{1}^+ \cdot I^-$ because the axial coordination of pyridine with the Fe center of $\mathbf{1}^+ \cdot I^-$ prevents aggregation. X-ray photoelectron spectroscopy (XPS) analysis of **1**/G clearly demonstrated that $\mathbf{1}^+$ was reduced by $1e^-$ in graphite to the neutral form **1** on the graphite surface [36]. Using a similar approach, here we prepared a supported catalyst (**1**/Vul) on Vulcan XC-72R, a well-known conductive carbon black, as shown schematically in Figure S1a. It should be mentioned that the adsorption of the catalyst molecule on Vulcan proceeded quantitatively under these reaction conditions, because the solution was almost colorless after heating Vulcan with $\mathbf{1}^+ \cdot I^-$ in pyridine.

It was difficult to detect the Fe peaks in the XPS spectrum of **1**/Vul, presumably because Vulcan XC-72R has a much larger surface area than graphite (254 vs. 3.9 m^2/g, see Table 1 and Figure S2 in the Supporting Information). Instead, we compared the Fe *K*-edge X-ray absorption near edge structure (XANES) of **1**/Vul, **1** deposited on silica gel (**1**/SiO_2), solid of **1**, $\mathbf{1}^+ \cdot I^-$ deposited on

TABLE 1 | Physical properties of carbon supports and the catalytic CH_4 oxidation activities of supported catalysts (**1**/Vul, **1**/KB, **1**/BP, **1**/AB, and **1**/G) at 25°C for 2 h. Values in parentheses indicate the S.D. of three independent experiments.

Carbon support / Catalyst	BET surface area [m^2 /g]	Particle size [nm]	[CH_3OH] [mM]	[CH_3OOH] [mM]	[HCHO] [mM]	[HCOOH] [mM]	MCN_{eff} for 2 h oxidation
Vulcan XC–72R / 1/Vul	254	30	0.18 (0.01)	0.69 (0.03)	0.09 (0.01)	1.13 (0.27)	107 (16)
Black Pearls 2000 / 1/BP	1475	15	0.10 (0.01)	0.72 (0.02)	0.04 (0.01)	1.17 (0.11)	117 (6)
Acetylene Black / 1/AB	51	35	0.09 (0.00)	0.69 (0.05)	0.02 (0.01)	0.47 (0.06)	72 (6)
Ketjen Black EC-DJ600 / 1/KB	1270	30	0.11 (0.01)	0.70 (0.02)	0.03 (0.00)	0.21 (0.05)	61 (3)
Graphite / 1/G	3.9	< 75 μm	0.02 (0.00)	0.04 (0.01)	0.00 (0.00)	0.00 (0.01)	4 (0)

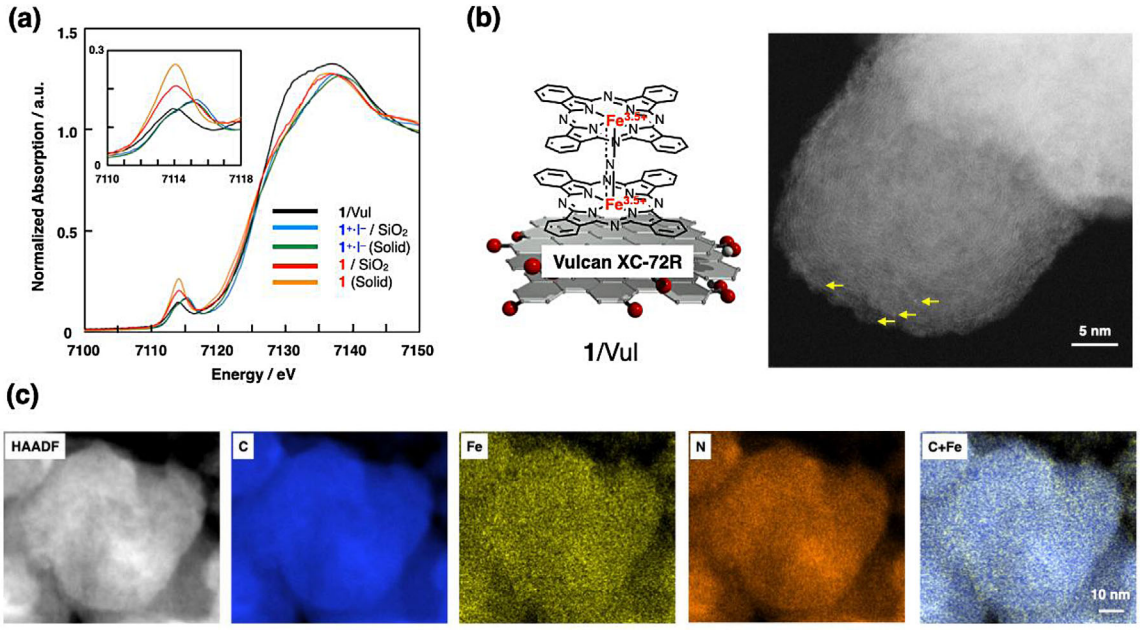

FIGURE 2 | Characterization of the Vulcan XC-72R-supported catalyst (**1**/Vul). (a) Fe *K*-edge XANES spectra of **1**/Vul and related materials (**1**, $\mathbf{1}^+\cdot I^-$, **1**/SiO_2, and $\mathbf{1}^+\cdot I^-/SiO_2$). Inset: expanded spectra of the pre-edge region. (b) HAADF-STEM image of **1**/Vul. The yellow arrows indicate spots assignable to **1** on the Vulcan support. (c) STEM-EDS mapping of **1**/Vul.

SiO_2 ($\mathbf{1}^+\cdot I^-/SiO_2$), and solid of $\mathbf{1}^+\cdot I^-$. The results are shown in Figure 2a. Their pre-edge peak tops are summarized in Table S1. The peak of **1**/Vul appears at a lower energy (7113.9 ev) than those of $\mathbf{1}^+\cdot I^-/SiO_2$ (7115.4 ev) and solid of $\mathbf{1}^+\cdot I^-$ (7115.2 ev) but almost identical to those of **1**/SiO_2 (7114.1 ev) and solid of **1** (7114.1v). These results indicate that $\mathbf{1}^+\cdot I^-$ was reduced by Vulcan during heating in pyridine and then deposited on the Vulcan surface in its neutral form (**1**). The high-angle annular dark-field scanning transmission electron microscopy (HAADF-STEM) image of **1**/Vul contains some bright spots on the layer-by-layer structure of Vulcan, which could be assigned to single μ-nitrido-bridged iron phthalocyanine dimers (Figure 2b). STEM-energy dispersive X-ray spectroscopy (EDS) mapping of iron and nitrogen indicated that the μ-nitrido-bridged iron phthalocyanine dimer was homogeneously dispersed over the carbon particle without forming large aggregates (Figure 2c). Also note that the EDS signal of iodine was very low (<0.01% in atomic fraction based on the EDS spectrum), further supporting that $\mathbf{1}^+\cdot I^-$ was reduced by Vulcan to **1** (Figure S3). It should also be noted that EDS analysis indicated trace Fe in pristine Vulcan XC-72R (Fe mass fraction = 0.078 ± 0.019). After deposition of **1** on Vulcan, the Fe mass fraction tended to get higher (0.145 ± 0.073), although the EDS quantification uncertainties were relatively large (page S7–S8 in the Supporting Information). These results do not alter the conclusions drawn from the HAADF-STEM/EDS results. It was also confirmed that pristine Vulcan XC-72R exhibited no apparent CH_4 oxidation activity at 25°C under the present conditions (vide infra).

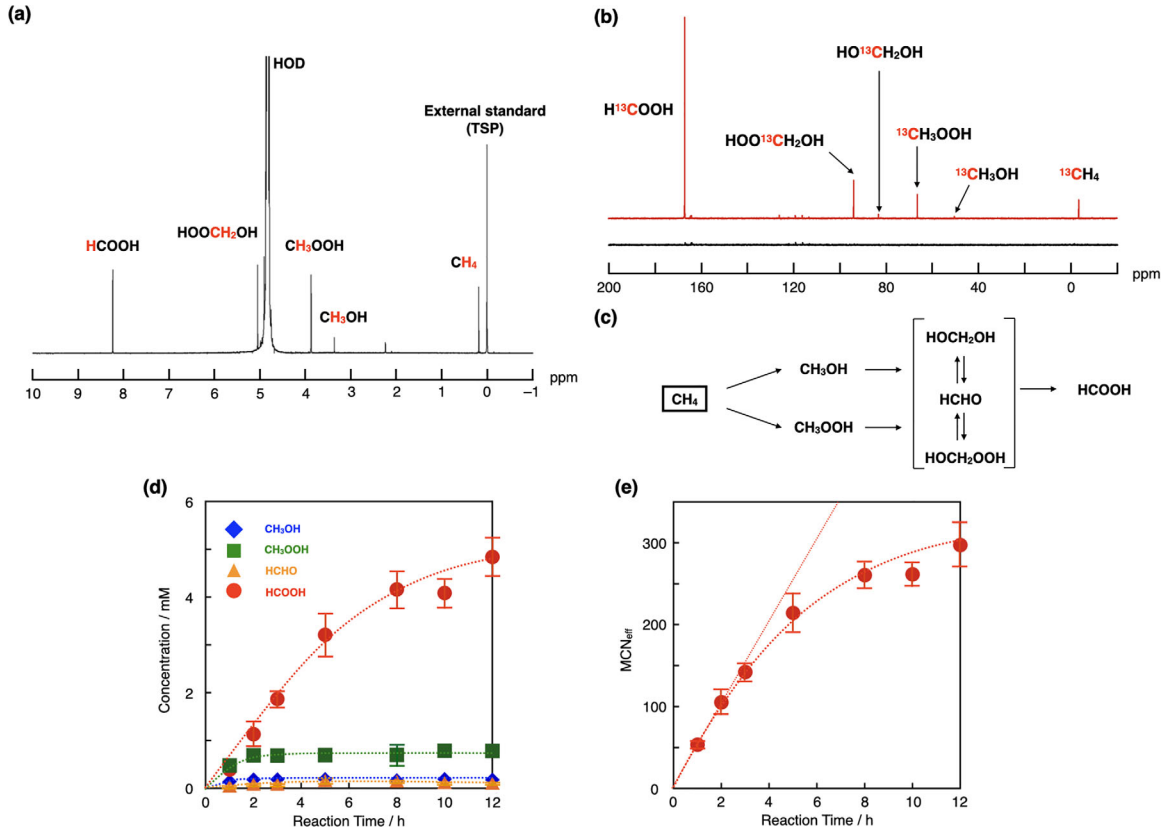

FIGURE 3 | CH_4 oxidation activity of **1**/Vul at 25°C. (a) ^{1}H-NMR spectrum of CH_4 reaction mixture. Reaction conditions: **1**/Vul (19 μM as **1**), 1.0 MPa of CH_4, D_2O (3.0 mL) containing excess H_2O_2 (189 mM) and TFA (51 mM), 25°C, and 2 h. (b) ^{13}C-NMR spectra of the reaction mixture using unlabeled CH_4 (black) and $^{13}CH_4$ (red). Reaction conditions: **1**/Vul (19 μM as **1**), 0.5 MPa of $^{13}CH_4$ or CH_4, D_2O (3.0 mL) containing excess H_2O_2 (189 mM) and TFA (51 mM), 25°C, and 2 h. (c) Stepwise oxidation of CH_4 by **1**/Vul in an acidic aqueous solution. Time dependence of (d) the concentration of C1 oxygenated products and (e) MCN_{eff} in the reaction of CH_4 over **1**/Vul at 25°C.

2.2 | Catalytic CH_4 Oxidation by 1/Vul at 25°C

We investigated the catalytic CH_4 oxidation activity of **1**/Vul (19 μM as **1**) at 25°C in an acidic aqueous solution (3.0 mL) containing 51 mM of trifluoroacetic acid (TFA) and 189 mM of H_2O_2 under a CH_4 atmosphere of 1.0 MPa, the same conditions we previously used to investigate **1**/G [36]. An acidic condition is necessary for efficient catalysis when using μ-nitrido-bridged iron phthalocyanine dimers, because this condition enhances the production of high-valent iron-oxo species by facilitating O—O bond cleavage of the corresponding hydroperoxo species (Scheme S1) [31–33]. The resulting solution was analyzed and quantified using gas chromatography-mass spectrometry (GC-MS) and ^{1}H-nuclear magnetic resonance (NMR) spectroscopy. Significant amounts of C1 oxygenated products, namely CH_3OH, CH_3OOH, HCHO (observed as $CH_2(OH)(OOH)$ and $CH_2(OH)_2$ in NMR), and HCOOH, were found in the solution as summarized in Figure 3a,d, and Table S2.

Upon replacing the CH_4 atmosphere with N_2, the amount of C1 oxygenated products became much smaller (see Table S2), indicating that they did not originate from the catalyst itself. ^{13}C-NMR spectrum of the reaction mixture using $^{13}CH_4$ as a substrate confirmed that these products came from CH_4 instead of from **1** or Vulcan (Figure 3b). The use of Vulcan XC-72R alone also afforded a very small amount of oxygenated products under the same reaction conditions (entries 17 and 18 in Table S2). It was also confirmed by the hot filtration experiment that the species on the Vulcan support actually showed the room-temperature CH_4 oxidation activity (see page S20–S21 in the Supporting Information). All these results suggest that **1** adsorbed on Vulcan efficiently catalyzed the CH_4 oxidation reaction. The small amount of oxidized products in the absence of CH_4 was presumably generated from organic solvents adsorbed on Vulcan and/or Vulcan itself (see Table S2).

The addition of excess Na_2SO_3 can effectively quench the reaction by •OH, whereas oxidation reactions mediated by high-valent iron-oxo species were reported to be only marginally affected by Na_2SO_3 [39–44]. However, in the case of CH_4 oxidation by **1**/Vul, excess Na_2SO_3 (100 mM) did not completely quench the reaction, even though it decreased the total amount of C1 oxygenated products to half of that before addition (entries 15 and 16, Table S2). We also applied electron paramagnetic resonance (EPR, Figure S4) and electrospray ionization time-of-flight mass spectrometry (ESI-TOF MS, Figure S8) analyses to the reaction mixture for CH_4 oxidation by **1**/Vul in the presence of excess 5,5-dimethyl-1-pyrroline (DMPO, 100 mM) as a radical scavenger. The amount of trapped •OH was much smaller compared to that of the C1 oxygenated products (Figure S7). These results suggest

that CH_4 oxidation via •OH is not dominant in this reaction system, and that the metal complex-based species should be the main reactive intermediate. Based on our previous MALDI-TOF MS experiment, which clearly showed the high-valent iron-oxo species of **1** (**1(oxo)**) after treating **1** deposited on a carbon surface with H_2O_2 [36], we assumed **1(oxo)** on Vulcan to be the most likely candidate for the reactive intermediate in the present system.

It is likely that CH_4 was oxidized in a stepwise manner in this acidic aqueous solution, as shown in Figure 3c. To discuss the activities of carbon-supported catalysts, we calculated the effective methane conversion number [MCN_{eff}, defined in Equations (1) and (2)] based on the concentrations of C1 oxygenated products in CH_4 and N_2 atmospheres. MCN_{eff} directly reflects the number of C—H bonds in CH_4 dissociated during the reaction.

$$MCN_{eff} = MCN_{(CH4)} - MCN_{(N2)} \quad (1)$$

$$MCN_{(CH4)}\ or\ MCN_{(N2)} = (C_{CH3OH} + C_{CH3OOH} + C_{HCHO} + C_{HCOOH})\,C_{Cat} \quad (2)$$

Next, we investigated the time courses of the concentration of C1 oxygenated products and MCN_{eff}, and the results are shown in Figure 3d,e, respectively. The initial linear increase in MCN_{eff} indicated that **1**/Vul worked stably under these reaction conditions. The gradual saturation of catalytic activity, especially after 2 h, was attributed to three reasons: (i) overoxidation of HCOOH [36, 45], (ii) consumption of H_2O_2 by the catalase reaction, as confirmed by our titration experiments (for details see Figure S9) [36, 46], and (iii) gradual deactivation of the catalyst. Regarding catalyst deactivation, we confirmed that after 4 h of reaction with CH_4, the activity of **1**/Vul decreased to almost 26% of the original value. Considering that the XANES spectra indicated that the catalyst after CH_4 oxidation retained similar oxidation states and coordination as the original one (Figure S10), the decreased catalytic activity afterwards is attributable to partial detachment of adsorbed **1** from the Vulcan surface. This assumption is also supported by the fact that the mass fraction of Fe in the catalyst after use (4 h reaction at 25°C), analyzed by EDS, was apparently decreased compared to that before use (see page S8 in the Supporting Information). Detached **1** from the Vulcan surface did not show apparent CH_4 oxidation activity in this reaction condition, as confirmed by the results of hot filtration experiments (see page S20–S21 in the Supporting Information).

Here, the initial reaction rate over **1**/Vul for the C—H bond activation of CH_4 at 25°C reached $MCN_{eff} = 1.5 \times 10^{-2}\ s^{-1}$ ($55\ h^{-1}$), as shown in Table S2 and Figure 3e. The ability of **1**/Vul to catalytically activate the C—H bond in CH_4 is considerably high among molecule-based CH_4 oxidation catalysts and even among general room-temperature CH_4 oxidation catalysts reported so far [17–30]. More importantly, from the viewpoint of SMCs or SIMCs, here we achieved a high catalytic CH_4 oxidation activity that is impossible for the metal complex or carbon substrate alone, by using an appropriate combination of μ-nitrido-bridged iron phthalocyanine dimer with a conductive carbon black support.

2.3 | Comparison of Catalytic CH_4 Oxidation Activities of 1/Vul and Fenton Reaction Using Fe^{2+} at 25°C

The Fenton reaction exhibits a high catalytic activity for the oxidative activation of C—H bonds in various organic pollutants under mild conditions. The most common Fenton reaction system uses Fe^{2+} and H_2O_2 in an acidic condition, where Fe^{2+} acts as a catalyst to produce •OH or ferryl iron from H_2O_2 as a reactive intermediate [47]. This system is both potent and simple because a strong oxidizing ability is obtained by mixing commercially available reagents without using any special equipment. Thus, it has long been used to treat wastewater and contaminated soil as "the last trump card". Under a condition similar to that of the Fenton reaction, we compared the catalytic C—H bond oxidation ability of **1**/Vul with that of the Fenton reaction using Fe^{2+}, using CH_4 as a substrate.

Wastewater treatment using the Fenton reaction of Fe^{2+} and H_2O_2 has an optimal pH of approximately 3 [47]. H_2SO_4 is often used to control the pH value here, and the catalytic activity tends to decrease at a lower pH. When we investigated the pH dependence of catalytic CH_4 oxidation by **1**/Vul at 25°C, the optimal pH was found to be 2 with TFA as an acid (Figure 4a and Table S5). This reaction also proceeded in the presence of H_2SO_4 as an acid at 25°C, and the catalytic activity was almost comparable to that in the presence of TFA at pH 3 (Table S6).

We performed ^{1}H-NMR measurements to compare the catalytic CH_4 oxidation activities of **1**/Vul (19 μM as **1**) and the Fenton reaction using Fe^{2+} (326 μM) at pH 3 and 25°C. Figure 4b shows the experimental results in D_2O (3.0 mL) solution containing excess H_2O_2 (50 μL of 35% H_2O_2, 189 mM) and H_2SO_4 (0.5 mM, pH ≈ 3) under a CH_4 pressure of 1.0 MPa for 2 h. In the case of the Fenton reaction, only a small amount of HCOOH (0.02 mM) was observed afterwards. In contrast, **1**/Vul produced a significant amount of C1 oxygenated compounds (0.11 mM of CH_3OH, 0.62 mM of CH_3OOH, 0.48 mM of HCHO, and 2.20 mM of HCOOH, as summarized in Table S6), even though much less catalyst was used (19 μM as **1** versus 326 μM of Fe^{2+}). Next, we tested the oxidation of CH_3OH, which is easier than CH_4 oxidation, in the Fenton reaction at 25°C. The reaction occurred catalytically (see Figure S11), suggesting that •OH or ferryl ion was actually generated in this condition. Meanwhile, EPR experiments in the presence of excess DMPO indicated that the amount of •OH trapped by DMPO was much larger in the Fenton reaction than in the reaction using **1**/Vul (Figures S5c, S6b, and S7), suggesting that highly reactive species other than •OH were involved in the oxidation by **1**/Vul. More importantly, **1**/Vul showed more potent C—H activation than the Fenton reaction under the same reaction conditions at 25°C.

2.4 | Discussion of the Reaction Mechanism

To investigate the reason for the high catalytic oxidation activity of **1**/Vul, we prepared other carbon-supported catalysts (**1**/KB, **1**/BP, and **1**/AB) using similar methods and commercially available conductive carbon blacks (Ketjen Black EC-DJ600 (KB), Black Pearls 2000 (BP), and Acetylene Black (AB)). In each case, 5.7 μmol of **1** was quantitatively adsorbed on 1.0 g of carbon

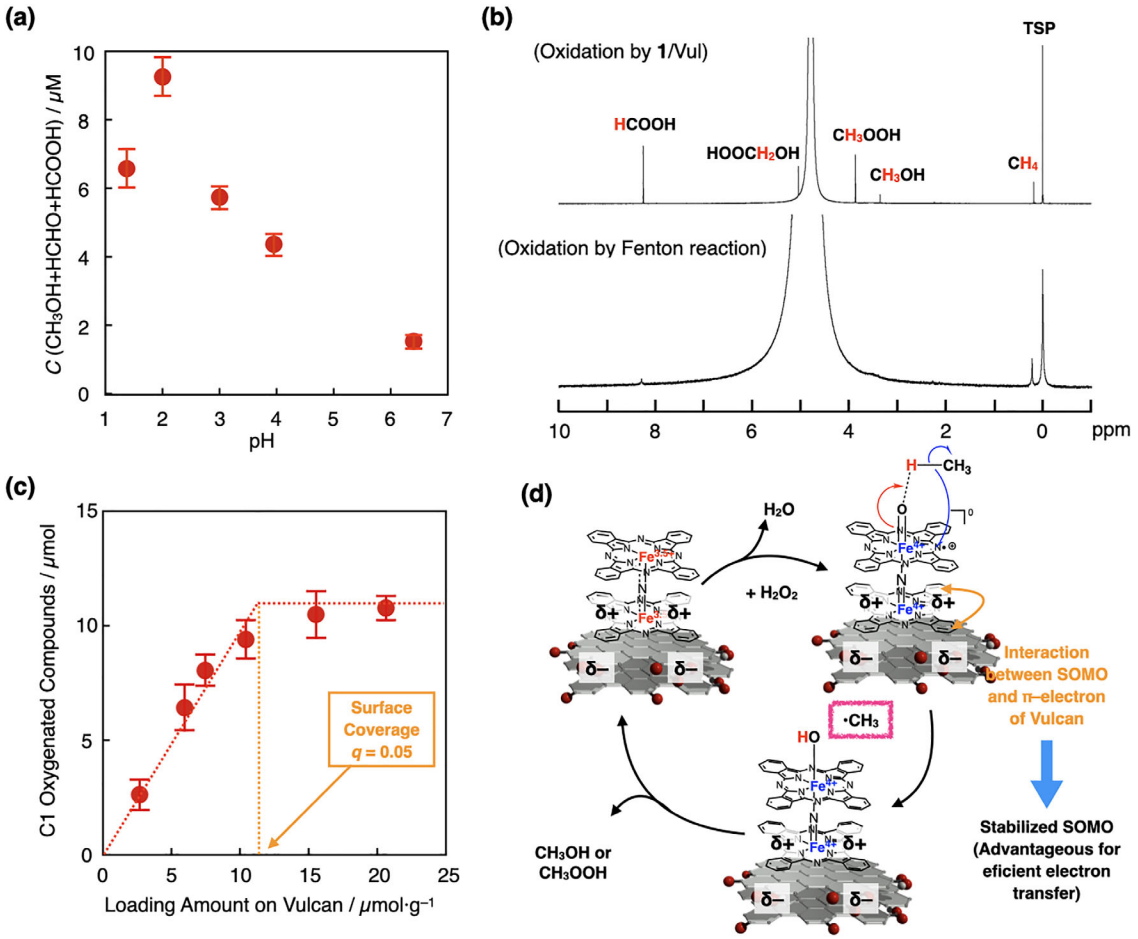

FIGURE 4 | Comparison of catalytic CH_4 oxidation activities of **1**/Vul and Fenton reaction at 25°C. (a) pH dependence in the catalytic CH_4 oxidation activity of **1**/Vul at 25°C. The pH values of the solution containing 51 mM of TFA were adjusted by the addition of aqueous NaOH. The details are shown in SI. (b) ^{1}H-NMR spectra of the CH_4 reaction mixtures with **1**/Vul (top) and $FeSO_4$ (bottom) at pH 3. Reaction conditions: 1.0 MPa CH_4, **1**/Vul (19 μM as **1**) or $FeSO_4$ (326 μM), D_2O (3.0 mL) containing H_2SO_4 (0.5 mM) and excess H_2O_2 (189 mM), 25°C, and 2 h. (c) Dependence of the total amount of C1 oxygenated products on the loading amount of **1** on Vulcan. (d) Proposed reaction mechanism of CH_4 oxidation over **1**/Vul. Error bars in (a) and (c) indicate the S.D. of three independent experiments.

support after heating in pyridine, as in the case of **1**/Vul. The catalytic CH_4 oxidation activities of **1**/Vul, **1**/KB, **1**/BP, **1**/AB, and **1**/G are summarized in Table 1. All of them showed significantly higher activity of **1** compared to that of **1**/G. However, the initial reaction rate (at 2 h of oxidation) seemed to depend on the type of carbon support, even though the loading of **1** was the same. Table 1 shows no apparent correlation between the catalytic CH_4 oxidation activity and the surface area or particle size of the carbon support. Rather, the catalytic activity of adsorbed **1** could have been affected by different electronic structures of the carbon blacks owing to variations in their structures. In fact, the Raman spectra indicate that the carbon blacks have considerably different I_D/I_G ratios from that of graphite (Figure S12), which is indicative of their structural differences [48].

To obtain further insight into the interaction between **1** and Vulcan, we prepared catalysts with different loadings of **1** per 1.0 g of Vulcan XC-72R and performed CH_4 oxidation experiments at 25°C. As shown in Figure 4c and Table S7, the total amount of C1 oxygenated products increased almost linearly at lower loadings but apparently became saturated at higher loadings. The highest catalytic activity was obtained at 11 μmol/g of **1**. Based on the Brunauer–Emmett–Teller (BET) surface area of Vulcan (254 m^2/g) and the molecular surface area of **1** (ca. 1.6 nm^2, Figure S13), the coverage (q) by **1** at this loading was calculated to be 0.05. This result suggests that the high catalytic activity is due to not only the simple stacking of **1** with the carbon surface but also the interaction between **1** and particular surface sites on Vulcan.

According to our previous density functional theory (DFT) calculations and electrochemical experiments, the stacking interaction of **1** with the π-surface of carbon material could cause a slight charge transfer due to interaction of the singly occupied molecular orbital (SOMO) of **1** with the π-orbital of carbon, which can lower the SOMO level of the catalyst [36]. This may be key to elucidating the role of Vulcan.

Figure 4d shows the proposed mechanism of CH_4 oxidation by **1**/Vul. Considering (1) the different optimal pH values between **1**/Vul and Fenton reaction as well as the much higher catalytic CH_4 oxidation activity of **1**/Vul with less •OH trapped by DMPO and (2) our previous MALDI-TOF MS observation of the high-valent iron-oxo species **1(oxo)** on a carbon substrate, the reaction of **1**/Vul could involve **1(oxo)** as the dominant reactive inter-

mediate. **1(oxo)** can efficiently activate the C—H bond of CH_4 via the PCET mechanism, in which both electrons and protons are extracted from CH_4 in a concerted manner [34, 35]. The enhanced catalytic ability of **1**/Vul could be explained by the electronic interaction with carbon, in particular, a lower SOMO of the high-valent iron-oxo species that promotes PCET with CH_4 and efficient formation of $\bullet CH_3$. Nevertheless, it is difficult to discuss the detailed mode of interaction between **1** and the Vulcan surface. In total, a series of C1 oxygenated products could be produced through oxidation by high-valent iron-oxo species instead of by •OH.

3 | Conclusions

We demonstrated that depositing the μ-nitrido-bridged iron phthalocyanine dimer **1** on an appropriate conductive carbon support dramatically enhanced its catalytic oxidation ability. The supported catalyst (**1**/Vul) achieved efficient C—H activation of CH_4 at 25°C in acidic aqueous solutions. Its catalytic ability exceeded that of the Fenton reaction using Fe^{2+} and H_2O_2, a system that has long been employed for wastewater treatment under the same conditions. We also demonstrated that the high catalytic activity of **1**/Vul occurs by the interaction of **1** with particular surface sites on Vulcan. It has been difficult for pure artificial high-valent iron-oxo-based molecular catalysts to achieve such a high CH_4 oxidation activity at room temperature. In SMCs or SIMCs, the activity of the molecular catalyst can be tuned through its interaction with the solid support. This strategy enables the modulation of interactions between the carbon surface and molecular metal complex-based catalysts to create novel catalysts for even more difficult reactions.

4 | Experimental Section

4.1 | Preparation of Supported Catalysts

In a typical experiment, the monocationic μ-nitrido-bridged iron phthalocyanine dimer $\mathbf{1}^+\cdot I^-$ (16.3 mg, 11.6 μmol as a pyridine adduct) was dissolved in pyridine (10 mL) to obtain a deep blue solution (Figure S1b). After adding a suspension of Vulcan XC-72R (1.93 g, Cabot Corp.) in pyridine (50 mL), the mixture was sonicated for 1 h. The resulting suspension was stirred for 20 h at 80°C. After filtration, the filtrate was almost colorless (Figure S1c). The separated solid was successively washed with pyridine (20 mL × 2) and CH_2Cl_2 (50 mL × 2) and dried under reduced pressure (~1 mmHg) at 80°C for 1 h.

The obtained solid was suspended in H_2O (50 mL) containing 5.0 mL of TFA and sonicated for 1 h. Then, the solid was separated by filtration and washed with H_2O to neutral pH. The purified solid was resuspended in H_2O (50 mL) containing 5.0 mL of TFA and sonicated for 1 h, followed by filtration again. The obtained solid was washed with H_2O to neutral pH and then dried under reduced pressure (~1 mmHg) at 80°C overnight. Finally, the solid was kept in air at room temperature until its weight became constant, giving **1**/Vul (1.87 g, Figure S1d). **1**/KB, **1**/BP, **1**/AB, and **1**/G were prepared similarly on different supports.

When mixing more than 11 μmol of $\mathbf{1}^+\cdot I^-$ with 1.0 g of Vulcan XC-72R, the color of the filtrate after heating at 80°C in pyridine remained deep blue. In these cases, the solvent was evaporated slowly to maximize the adsorption of remaining catalyst molecules in the solvent on Vulcan. After evaporation, the same washing procedure was performed as described above.

4.2 | CH_4 Oxidation Reactions

CH_4 oxidation was performed in a stainless-steel autoclave with a glass tube. A mixture of a solid-supported catalyst (10 mg, 19 μM as **1**), TFA (12 μL, 51 mM), and 35% H_2O_2 aq. (50 μL, 189 mM) in H_2O (3.0 mL) was stirred by using a magnetic stirring bar at 25°C in a water bath or an oil bath under a CH_4 atmosphere of 1.0 MPa for a given reaction time. After the reaction mixture was filtered through a disposable membrane filter (ADVANTEC, DISMIC-13CP), the resulting filtrate was mixed with an appropriate amount of an aqueous isovaleric acid solution (100 mM) and analyzed by GC-MS (system: Shimadzu GCMS-QP2020, detection: EI, column: Agilent DB-WAX UI, external standard: isovaleric acid (5 mM), temperature conditions: initial: 50°C—hold (1 min)—raise to 220°C (10°C/min)— hold (5 min)). The yields of CH_3OH and HCOOH were determined based on the results of GC-MS.

The yield of HCHO was determined using the method reported by Yu et al. [49]. Typically, 25 μL of the filtrate obtained from the reaction mixture was diluted with 50 mL of H_2O, followed by the addition of an aqueous solution (469 μM) of PFBOA·HCl (3.0 mL). The resulting mixture was stirred for 2 h. Then, sulfuric acid (1+1) (0.8 mL), NaCl (20 g), and hexane (5.0 mL) were added, and the mixture was stirred vigorously for 5 min. The separated organic layer was dried over anhydrous Na_2SO_4. A mixture of the resulting solution (1.0 mL) and a 1.0 mM 1-chlorodecane/hexane solution (10.1 μL) was analyzed by GC-MS (Agilent 7890A equipped with JEOL JMS-T100GCV, detection: EI, column: Agilent DB-WAX UI, external standard: 1-chlorodecane (10 μM), temperature conditions: initial: 70°C—hold (10 min)—raise to 150°C (10°C/min)—raise to 240°C (30°C/min)—hold (3 min)). In an acidic aqueous solution, HCHO can be hydroxylated to $CH_2(OH)_2$. In addition, ^{13}C-NMR study of the reaction mixture of the $^{13}CH_4$ oxidation reaction (see Supporting Information) by the catalysts used in this study indicated that $H_2C(OH)(OOH)$ was produced as one of the major C1 oxygenated products. It is considered that both $H_2C(OH)(OOH)$ and $H_2C(OH)_2$ can be converted into the same oxime through the derivatization reaction with the reaction PFBOA·HCl mentioned above.

It was reported that CH_3OOH was difficult to be quantified by GC-MS because it can easily be decomposed [45]. Therefore, CH_3OOH was quantified by using ^{1}H-NMR measurement as mentioned below: A mixture of a solid-supported catalyst (10 mg, 19 μM as **1**), TFA (12 μL, 51 mM), and 35% H_2O_2 aq. (50 μL, 189 mM) in D_2O (3.0 mL), was stirred by using a magnetic stirring bar at 25°C in a water bath or an oil bath under a CH_4 atmosphere of 1.0 MPa for a given reaction time. After the reaction mixture was filtered through a disposable membrane filter (ADVANTEC, DISMIC-13CP), the resulting filtrate was subjected to ^{1}H-NMR measurements using a JEOL JNM-ECS400 (400 MHz for ^{1}H) spectrometer. 3-(Trimethylsilyl)-

2,2,3,3-tetradeuteropropionic acid sodium salt (TSP, 10 mM in D_2O) in a glass capillary was used as an external standard. The concentration of CH_3OOH was determined based on the integration of TSP.

The evaluations of the CH_4 oxidation reactions using **1**/KB, **1**/BP, **1**/AB, **1**/G, and Vulcan XC-72R (with no catalyst molecule) were performed in a similar manner. The reactions in the presence of 100 mM Na_2SO_3 (entries 15 and 16 in Table S2) were performed in a similar manner.

Acknowledgments

We are grateful for fruitful discussions with Dr. Atsushi Ogawa and Dr. Yuya Shimizu from Okumura Corporation, Prof. Osami Shoji from Nagoya University, and Prof. Satoru Takakusagi from Hokkaido University. We thank Mr. Kouichi Okudaira for his contribution to the HAADF-STEM/EDS analyses. XAFS measurements were performed with the approval of PF-PAC (Nos. 2023G161 and 2023G162) and the Aichi Synchrotron Radiation Center (No. 202304025). KT was financially supported by a JSPS KAKENHI Grant-in-Aid for Challenging Research (Exploratory) (No. JP25K22271), and YY was financially supported by a Grant-in-Aid for Scientific Research (B) (No. JP25K01843) and a Grant-in-Aid for Transformative Research Areas (A) "Green Catalysis Science" (No. JP24H01844). MT was financially supported by a Grant-in-Aid for International Leading Research (No. JP23K020034). KH was finacially supported by a Grant-in-Aid for Transformative Research Areas (A) "Materials Science of Meso-Hierarchy" (No. JP23H04874). This study was also supported by the Okumura Corporation and "Quantum-Based Frontier Research Hub for Industry Development", Nagoya University, Japan.

Conflicts of Interest

The authors declare no conflict of interest.

Supporting Information

Detailed experimental conditions and methods, synthesis details of all catalysts, and additional experimental details/materials/methods/data are presented within the Supporting Information.

Data Availability Statement

The data that support the findings of this study are available from the corresponding author upon reasonable request.

References

1. X. Cui, W. Li, P. Ryabchuk, K. Junge, and M. Beller, "Bridging Homogeneous and Heterogeneous Catalysis by Heterogeneous Single-Metal-Site Catalysts," *Nature Catalysis* 11 (2018): 385–397.

2. S. Mitchell and J. Pérez-Ramírez, "Single Atom Catalysis: a Decade of Stunning Progress and the Promise for a Bright Future," *Nature Communications* 11 (2020): 4302, https://doi.org/10.1038/s41467-020-18182-5.

3. M. B. Gawande, P. Fornasiero, and R. Zboˆril, "Carbon-Based Single-Atom Catalysts for Advanced Applications," *ACS Catalysis* 10 (2020): 2231–2259, https://doi.org/10.1021/acscatal.9b04217.

4. J. Li, C. Chen, L. Xu, et al., "Challenges and Perspectives of Single-Atom-Based Catalysts for Electrochemical Reactions," *JACS Au* 3 (2023): 736–755, https://doi.org/10.1021/jacsau.3c00001.

5. V. B. Saptal, V. Ruta, M. A. Bajada, and G. Vilé, "Single-Atom Catalysis in Organic Synthesis," *Angewandte Chemie International Edition* 62 (2023): e202219306, https://doi.org/10.1002/anie.202219306.

6. Q. Fu, H. Saltsburg, and M. Flytzani-Stephanopoulos, "Active Nonmetallic Au and Pt Species on Ceria-Based Water-Gas Shift Catalysts," *ScienceScience* 301 (2003): 935–938, https://doi.org/10.1126/science.1085721.

7. R. Bashyam and P. Zelenay, "A Class of Non-Precious Metal Composite Catalysts for Fuel Cells," *NatureNature* 443 (2006): 63–66, https://doi.org/10.1038/nature05118.

8. K. Saini, A. N. Nair, A. Yadav, et al., "Nickel-Based Single-Molecule Catalysts With Synergistic Geometric Transition and Magnetic Field-Assisted Spin Selection Outperform RuO_2 for Oxygen Evolution," *Advanced Energy Materials* 13 (2023): 2302170, https://doi.org/10.1002/aenm.202302170.

9. J. Lu, C. Aydin, A. J. Liang, C.-Y. Chen, N. D. Browning, and B. C. Gates, "Site-Isolated Molecular Iridium Complex Catalyst Supported in the 1-Dimensional Channels of Zeolite HSSZ-53: Characterization by Spectroscopy and Aberration-Corrected Scanning Transmission Electron Microscopy," *ACS Catalysis* 2 (2012): 1002–1012, https://doi.org/10.1021/cs300139p.

10. V. Georgakilas, J. A. Perman, J. Tucek, and R. Zboril, "Broad Family of Carbon Nanoallotropes: Classification, Chemistry, and Applications of Fullerenes, Carbon Dots, Nanotubes, Graphene, Nanodiamonds, and Combined Superstructures," *Chemical Reviews* 115 (2015): 4744, https://doi.org/10.1021/cr500304f.

11. D. S. Su, S. Perathoner, and G. Centi, "Nanocarbons for the Development of Advanced Catalysts," *Chemical Reviews* 113 (2013): 5782, https://doi.org/10.1021/cr300367d.

12. K. Chen, K. Liu, P. An, et al., "Iron Phthalocyanine With Coordination Induced Electronic Localization to Boost Oxygen Reduction Reaction," *Nature Communications* 11 (2020): 4173, https://doi.org/10.1038/s41467-020-18062-y.

13. P. Schwach, X. Pan, and X. Bao, "Direct Conversion of Methane to Value-Added Chemicals Over Heterogeneous Catalysts: Challenges and Prospects," *Chemical Reviews* 117 (2017): 8497, https://doi.org/10.1021/acs.chemrev.6b00715.

14. M. Ravi, M. Ranocchiari, and J. A. van Bokhoven, "The Direct Catalytic Oxidation of Methane to Methanol—A Critical Assessment," *Angewandte Chemie International Edition* 56 (2017): 16464–16483, https://doi.org/10.1002/anie.201702550.

15. N. F. Dummer, D. J. Willock, Q. He, et al., "Methane Oxidation to Methanol," *Chemical Reviews* 123 (2023): 6359–6411, https://doi.org/10.1021/acs.chemrev.2c00439.

16. H. Fujisaki and T. Kojima, "Functionalization of Methane Using Molecular Metal Complexes as Catalysts," *Catalysis Science & Technology* 13 (2023): 4270–4284, https://doi.org/10.1039/D3CY00647F.

17. E. V. Starokon, M. V. Parfenov, L. V. Pirutko, S. I. Abornev, and G. I. Panov, "Room-Temperature Oxidation of Methane by α-Oxygen and Extraction of Products From the FeZSM-5 Surface," *The Journal of Physical Chemistry C* 115 (2011): 2155–2161, https://doi.org/10.1021/jp109906j.

18. M. V. Parfenov, E. V. Starokon, L. V. Pirutko, and G. I. Panov, "Quasicatalytic and Catalytic Oxidation of Methane to Methanol by Nitrous Oxide Over FeZSM-5 Zeolite," *Journal of Catalysis* 318 (2014): 14–21, https://doi.org/10.1016/j.jcat.2014.07.009.

19. B. E. R. Snyder, P. Vanelderen, M. L. Bols, et al., "The Active Site of Low-Temperature Methane Hydroxylation in Iron-Containing Zeolites," *Nature* 536 (2016): 317–321, https://doi.org/10.1038/nature19059.

20. N. Agarwal, S. J. Freakley, R. U. McVicker, et al., "Aqueous Au-Pd Colloids Catalyze Selective CH_4 Oxidation to CH_3OH With O_2 Under Mild Conditions," *Science* 358 (2017): 223–227, https://doi.org/10.1126/science.aan6515.

21. X. Cui, H. Li, Y. Wang, et al., "Room-Temperature Methane Conversion by Graphene-Confined Single Iron Atoms," *Chemistry (Weinheim An Der Bergstrasse, Germany)* 4 (2018): 1902–1910, https://doi.org/10.1016/j.chempr.2018.05.006.

22. E. Tabor, J. Dedecek, K. Mlekodaj, Z. Sobalik, P. C. Andrikopoulos, and S. Sklenak, "Dioxygen Dissociation Over Man-Made System at Room Temperature to Form The Active a-Oxygen For Methane Oxidation," *Science Advances* 6 (2020): eaaz9776, https://doi.org/10.1126/sciadv.aaz9776.

23. M. L. Bols, J. Devos, H. M. Rhoda, et al., "Selective Formation of α-Fe(II) Sites on Fe-Zeolites Through One-Pot Synthesis," *Journal of the American Chemical Society* 143 (2021): 16243–16255, https://doi.org/10.1021/jacs.1c07590.

24. Y. Xing, Z. Yao, W. Li, et al., "Fe/Fe_3 C Boosts H_2O_2 Utilization for Methane Conversion Overwhelming O_2 Generation," *Angewandte Chemie International Edition* 60 (2021): 8889–8895, https://doi.org/10.1002/anie.202016888.

25. J. Mao, H. Liu, X. Cui, et al., "Direct Conversion of Methane With O_2 at Room Temperature Over Edge-Rich MoS_2," *Nature Catalysis* 6 (2023): 1052–1061, https://doi.org/10.1038/s41929-023-01030-2.

26. A. Hu, J.-J. Guo, H. Pan, and Z. Zuo, "Selective Functionalization of Methane, Ethane, and Higher Alkanes by Cerium Photocatalysis," *ScienceScience* 361 (2018): 668–672, https://doi.org/10.1126/science.aat9750.

27. C. Han, Y. Cao, W. Yu, et al., "Selective Cleavage of Chemical Bonds in Targeted Intermediates for Highly Selective Photooxidation of Methane to Methanol," *Journal of the American Chemical Society* 145 (2023): 8609–8620, https://doi.org/10.1021/jacs.3c01317.

28. H. Sato, A. Ishikawa, H. Saito, T. Higashi, K. Takeyasu, and T. Sugimoto, "Critical Impacts of Interfacial Water on C–H Activation in Photocatalytic Methane Conversion," *Communications Chemistry* 6 (2023): 8, https://doi.org/10.1038/s42004-022-00803-3.

29. J. Ding, Z. Teng, X. Su, et al., "Asymmetrically Coordinated Cobalt Single Atom on Carbon Nitride for Highly Selective Photocatalytic Oxidation of CH4 to CH3OH," *Chemistry (Weinheim An Der Bergstrasse, Germany)* 9 (2023): 1017–1035, https://doi.org/10.1016/j.chempr.2023.02.011.

30. S. I. Chan, Y.-J. Lu, P. Nagababu, et al., "Efficient Oxidation of Methane to Methanol by Dioxygen Mediated by Tricopper Clusters," *Angewandte Chemie International Edition* 52 (2013): 3731–3735, https://doi.org/10.1002/anie.201209846.

31. P. Afanasiev and A. B. Sorokin, "μ-Nitrido Diiron Macrocyclic Platform: Particular Structure for Particular Catalysis," *Accounts of Chemical Research* 49 (2016): 583–593, https://doi.org/10.1021/acs.accounts.5b00458.

32. A. B. Sorokin, E. V. Kudrik, and D. Bouchu, "Bio-Inspired Oxidation of Methane in Water Catalyzed by N-Bridged Diiron Phthalocyanine Complex," *Chemical Communications* 22 (2008): 2562–2564, https://doi.org/10.1039/b804405h.

33. Ü. Í¸sci, A. S. Faponle, P. Afanasiev, et al., "Chemical and Phase Evolution of Amorphous Molybdenum Sulfide During the Hydrogen Evolution Reaction: A Combined Operando and In Silico Study," *Chemical Science* 6 (2015): 5063–5075.

34. M. H. V. Huynh and T. J. Meyer, "Proton-Coupled Electron Transfer," *Chemical Reviews* 107 (2007): 5004–5064, https://doi.org/10.1021/cr0500030.

35. J. E. M. N. Klein and G. Knizia, "cPCET Versus HAT: A Direct Theoretical Method for Distinguishing X–H Bond-Activation Mechanisms," *Angewandte Chemie International Edition* 57 (2018): 11913–11917, https://doi.org/10.1002/anie.201805511.

36. Y. Yamada, K. Morita, T. Sugiura, et al., "Stacking of a Cofacially Stacked Iron Phthalocyanine Dimer on Graphite Achieved High Catalytic CH4 Oxidation Activity Comparable to That of pMMO," *JACS Au* 3 (2023), 823–833.

37. H. P. Boehm, "Some Aspects of the Surface Chemistry of Carbon Blacks and Other Carbons," *Carbon* 32 (1994): 759–769, https://doi.org/10.1016/0008-6223(94)90031-0.

38. L.-H. Zhang, Y. Shi, Y. Wang, and N. R. Shiju, "Nanocarbon Catalysts: Recent Understanding Regarding the Active Sites," *Advancement of Science* 7 (2020): 1902126, https://doi.org/10.1002/advs.201902126.

39. C. Hammond, M. M. Forde, M. H. Ab Rahim, et al., "Direct Catalytic Conversion of Methane to Methanol in an Aqueous Medium by Using Copper-Promoted Fe-ZSM-5," *Angewandte Chemie International Edition* 51 (2012): 5129–5133, https://doi.org/10.1002/anie.201108706.

40. Y. Yamada, J. Kura, Y. Toyoda, and K. Tanaka, "μ-Nitrido-Bridged Iron Phthalocyanine Dimer Bearing Eight Peripheral 12-Crown-4 Units and Its Methane Oxidation Activity," *New Journal of Chemistry* 44 (2020): 19179–19183, https://doi.org/10.1039/D0NJ04601A.

41. Y. Yamada, Y. Miwa, Y. Toyoda, T. Yamaguchi, S. Akine, and K. Tanaka, "Synthesis of a Monocationic M-Nitrido-Bridged Iron Porphycene Dimer and Its Methane Oxidation Activity," *Dalton Transactions* 50 (2021): 16775–16781, https://doi.org/10.1039/D1DT02922C.

42. Y. Yamada, J. Kura, Y. Toyoda, and K. Tanaka, "High Catalytic Methane Oxidation Activity of Monocationic M-Nitrido-Bridged Iron Phthalocyanine Dimer With Sixteen Methyl Groups," *Dalton Transactions* 50 (2021): 6718–6724, https://doi.org/10.1039/D1DT00941A.

43. Y. Yamada, Y. Miwa, Y. Toyada, Q. M. Phung, K. Oyama, and K. Tanaka, "Evaluation of CH 4 Oxidation Activity of High-Valent Iron-Oxo Species of a M-Nitrido-Bridged Heterodimer of Iron Porphycene and Iron Phthalocyanine," *Catalysis Science & Technology* 13 (2023): 1725–1734, https://doi.org/10.1039/D2CY01980A.

44. Y. Yamada, Y. Miwa, Y. Toyoda, Y. Uno, Q. M. Phung, and K. Tanaka, "Effect of Porphyrin Ligands on the Catalytic CH 4 Oxidation Activity of Monocationic M-Nitrido-Bridged Iron Porphyrinoid Dimers by Using H 2 O 2 as an Oxidant," *Dalton Transactions* 53 (2024): 6556–6567, https://doi.org/10.1039/D3DT04313D.

45. M. M. Forde, B. C. Grazia, R. Armstrong, et al., "Methane Oxidation Using Silica-Supported N-Bridged Di-Iron Phthalocyanine Catalyst," *Journal of Catalysis* 290 (2012): 177–185, https://doi.org/10.1016/j.jcat.2012.03.013.

46. A. Ghosh, D. A. Mitchell, A. Chanda, et al., "Catalase−Peroxidase Activity of Iron(III)−TAML Activators of Hydrogen Peroxide," *Journal of the American Chemical Society* 130 (2008): 15116–15126, https://doi.org/10.1021/ja8043689.

47. D. Bury, M. Jakubczak, J. Bogacki, P. Marcinowski, and A. Jastrzębska, *Wastewater Treatment With the Fenton Process, Principles and Applications* (CRC Press, 2024).

48. A. Sadezky, H. Muckenhuber, H. Grothe, R. Niessner, and U. Pöschl, "Raman Microspectroscopy of Soot and Related Carbonaceous Materials: Spectral Analysis and Structural Information," *CarbonCarbon* 43 (2005): 1731–1742, https://doi.org/10.1016/j.carbon.2005.02.018.

49. S. S. H. Ho and J. Z. Yu, "Feasibility of Collection and Analysis of Airborne Carbonyls by on-Sorbent Derivatization and Thermal Desorption," *Analytical Chemistry* 74 (2002): 1232–1240, https://doi.org/10.1021/ac015708q.

Supporting Information

Additional supporting information can be found online in the Supporting Information section.

Supporting File: cctc70565-supp-0001-SuppMat.pdf.